

# UC Riverside

## UC Riverside Previously Published Works

### Title

Nitrate subsurface transport and losses in response to its initial distributions in sloped soils: An experimental and modelling study

### Permalink

<https://escholarship.org/uc/item/29s072q1>

### Journal

Hydrological Processes, 33(26)

### ISSN

0885-6087

### Authors

Xie, Meixiang  
Šimůnek, Jirka  
Zhang, Zhanyu  
[et al.](#)

### Publication Date

2019-12-30



### DOI

10.1002/hyp.13556

Peer reviewed

## RESEARCH ARTICLE

# Nitrate subsurface transport and losses in response to its initial distributions in sloped soils: An experimental and modelling study

Meixiang Xie<sup>1,2</sup> | Jirka Šimůnek<sup>3</sup>  | Zhanyu Zhang<sup>1,2</sup>  | Pingcang Zhang<sup>4</sup> |  
Jinxin Xu<sup>4</sup> | Qingming Lin<sup>4</sup>

<sup>1</sup>College of Water Conservancy and Hydropower Engineering, Hohai University, Nanjing, China

<sup>2</sup>College of Agricultural Engineering, Hohai University, Nanjing, China

<sup>3</sup>Department of Environmental Sciences, University of California, Riverside, CA, USA

<sup>4</sup>Department of Soil and Water Conservation, Changjiang River Scientific Research Institute, Wuhan, China

## Correspondence

Zhanyu Zhang, College of Water Conservancy and Hydropower Engineering, Hohai University, Nanjing 210098, China.  
Email: zhanyu\_hhu@163.com

## Funding information

China Scholarship Council; Fundamental Research Funds for the Central Universities, Grant/Award Number: 2018B627X14; National Natural Science Foundation of China, Grant/Award Number: 51879071; Postgraduate Research & Practice Innovation Program of Jiangsu Province, Grant/Award Number: KYCX18\_0596; Priority Academic Program Development of Jiangsu Higher Education Institutions, Grant/Award Number: YS111001; Changjiang River Scientific Research Institute

## Abstract

Transport and losses of nitrate from sloped soils are closely linked to nitrogen fertilizer management. Previous studies have always focused on different types of fertilizer applications and rarely analysed various initial nitrate distributions as a result of nitrogen fertilizer applications. Under certain conditions, both subsurface lateral saturated flow and vertical leaching dominate nitrate losses. Soil tank experiments and HYDRUS-2D modelling were used to better understand the subsurface nitrate transport and losses through lateral saturated flow and vertical leaching under various initial nitrate distributions. Low (L: 180 mg L<sup>-1</sup>), normal (N: 350 mg L<sup>-1</sup>), and high (H: 500 mg L<sup>-1</sup>) nitrate concentrations were used in five different distributions (NNNN, NLLN, LHHL, LNLN, and HHHN) along the slope of the tank. The first two treatments (NNNN and NLLN) were analysed both experimentally and numerically. Experiments were conducted under 12 rainfall events at intervals of 3 days. The HYDRUS-2D model was calibrated and validated against the experimental data and demonstrated good model performance. The other three treatments (LHHL, LNLN, and HHHN) were investigated using the calibrated model. Nitrate concentrations in purple sloped soils declined exponentially with time under intermittent rainfalls, predominantly in the upper soil layers. Non-uniform initial nitrate distributions contributed to larger differences between four locations along the slope in deeper soil layers. The non-uniform nitrate distribution either enhanced or reduced decreases in nitrate concentrations in areas with higher or lower initial nitrate concentrations, respectively. Higher nitrate concentrations at the slope foot and along the slope were reduced mainly by lateral flow and vertical leaching, respectively. Increasing nitrogen application rates increased subsurface nitrate losses. Mean subsurface lateral nitrate fluxes were twice as large as mean vertical leaching nitrate fluxes. However, due to longer leaching durations, total nitrate losses due to vertical leaching were comparable with those due to lateral flow, which indicated comparable environmental risks to surface waters and groundwater.

## KEYWORDS

HYDRUS-2D, initial nitrate concentration distributions, intermittent rainfall, sloped soils, subsurface lateral flow, vertical leaching

## 1 | INTRODUCTION

Sloped soils occupy two thirds of the land area in China. As such, sloping farmlands play an important role in agricultural production (Xie, Zhang, Zhang, Xu, & Lin, 2018). Specifically, purple sloped soils account for more than 70% of the farmland in the south-west of China (Ma et al., 2016). Due to its low cost, urea fertilizer is currently the most favoured form of nitrogen fertilizer utilized in agricultural production (Prasertsak et al., 2002). It is well known that excessive fertilizer applications cause nutrient leaching and losses towards groundwater. Nitrate loss from sloped soils has been increasingly recognized as a source of serious pollution in the water environment (Xie et al., 2018; Zhang, Tang, Gao, & Zepp, 2011).

Nitrate is usually lost from sloped soils after rainfalls mainly due to subsurface outflow and also through leaching towards deep groundwater. A large number of studies have shown that subsurface flow dominates nitrate losses from sloped soils (Bechmann, 2014; Jia, Lei, Lei, Ye, & Zhao, 2007; Wang, Zhang, Lin, & Zepp, 2011; Zheng, Liu, Zuo, Wang, & Nie, 2017). Because purple sloped soils were formed by rock weathering, subsurface lateral flow is abundant at the interface between the soil and the bedrock, which have dramatically different permeabilities (Baram et al., 2016; Tang et al., 2012). Hence, nitrate dissolved in water is easily lost through subsurface lateral flow. Moreover, leaching towards deep zones also plays an important role in nitrate losses (Baram et al., 2016; Filipovic, Toor, Ondrasek, & Kodesova, 2015; Kahl et al., 2007). However, studies of nitrate losses from purple sloped soils rarely take into account vertical nitrate leaching to deep groundwater.

Spatial and temporal variabilities in  $\text{NO}_3\text{-N}$  concentrations significantly affect nitrate transport and losses in soils. Filipovic et al. (2015) reported that a large percentage of nitrate fertilizer can reach the bottom of the soil profile and leach into groundwater. Zhu et al. (2009) found that the maximum  $\text{NO}_3\text{-N}$  concentrations appeared in the upper soil layers at the foot of the purple soil hillslope. Nitrate transfer in soils is dominated by the spatial variability of physical and chemical soil properties and by the spatial and temporal variabilities of water and fertilizer applications (Baram et al., 2016).

Rainfall factors such as intensity and duration play a crucial role in nitrate losses from sloped soils (Kleinman et al., 2006; Wu, Peng, Qiao, & Ma, 2018). Additionally, slope gradients (Komatsu et al., 2018; Wu et al., 2018) and fertilizer management (Sweeney, Pierzynski, & Barnes, 2012) also have great impacts on nitrate losses. In the past, researchers analysed effects of fertilizer management on nitrate losses mainly by means of application rates (Delgado, Khosla, Bausch, Westfall, & Inman, 2005; Russo, Tully, Palm, & Neill, 2017; Wang, Ying, Yin, Zheng, & Cui, 2018), fertilizer types (Liu, Yang, Yang, & Zou, 2012; Nyamangara, Bergstrom, Piha, & Giller, 2003; Smith, Owens, Leytem, & Warnemuende, 2007), placement locations (Prasertsak et al., 2002; Wang, Ping, Pan, & Shen, 2012), and fertilizer application techniques (Ke et al., 2018; Zhao & Shao, 2002). Russo et al. (2017) reported that porewater nitrate concentrations and leaching fluxes are highest at locations with highest applications of nitrogen fertilizer.

Wang et al. (2012) found that bromine losses due to run-off are prone to happen when the solute is placed on the surface of the slope foot. Prasertsak et al. (2002) reported that incorporating urea into the soil rather than spreading it on the surface reduced ammonia nitrogen losses from 37.3% to 5.5% of applied nitrogen. These different nitrogen fertilizer application rates and placements cause different initial nitrate distributions in soils, which in turn impact the nitrate transport and losses. Hence, different initial nitrate distributions as a result of various fertilizer applications play a crucial role in nitrate losses. However, direct effects of initial nitrate spatial distributions on nitrate transport and losses are rarely addressed in the literature.

Subsurface nitrate transport and losses accompanied by subsurface water flow are complex processes (Zhu et al., 2009). It is still a challenge to fully understand the relation between subsurface nitrate transport and losses and subsurface water flow. Visual modelling software is a useful tool for visualizing and identifying the subsurface nitrate transport subjected to various initial nitrate distributions. HYDRUS-2D software has been widely used in the literature in studies of subsurface nitrogen dynamics and leaching in croplands (Doltra & Munoz, 2010; Karandish & Šimůnek, 2017; Salehi, Navabian, Varaki, & Pirmoradian, 2017). For example, Karandish and Šimůnek (2017) highlighted that HYDRUS-2D was capable of simulating subsurface water and nitrogen dynamics under different irrigation scenarios. Also, Salehi et al. (2017) reported that HYDRUS-2D well assessed the relationship between fertilizer applications and nitrate leaching in subsurface controlled drainage for a physical model of paddy fields. Because many other successful HYDRUS-2D applications have been reported by Šimůnek, van Genuchten, and Šejna (2016), we use this modelling software to simulate complex processes of the subsurface nitrate transport and losses in sloped soils under various initial nitrate distributions.

To improve our understanding and interpretation of subsurface nitrate transport and losses under various nitrate distributions, we conducted both laboratory experiments and numerical simulations using the HYDRUS-2D modelling software. In particular, spatial and temporal distributions of porewater  $\text{NO}_3\text{-N}$  concentrations in purple sloped soils and nitrogen losses through subsurface lateral saturated flow and vertical leaching were evaluated. In particular, the effects of water flow and initial nitrate distributions on its transport and losses were studied. Furthermore, relations between the subsurface nitrate transport and losses, and differences in  $\text{NO}_3\text{-N}$  losses due to lateral saturated flow and vertical leaching, were analysed to better understand subsurface  $\text{NO}_3\text{-N}$  losses from sloped soils.

## 2 | MATERIALS AND METHODS

### 2.1 | Laboratory experiments

#### 2.1.1 | Experimental set-up and design

Two 200-cm-long, 50-cm-deep, and 50-cm-wide steel soil tanks were used for laboratory experiments (Figure 1). At the bottom of one tank, a 10-cm-deep cement layer was set up to imitate aquitard bedrock

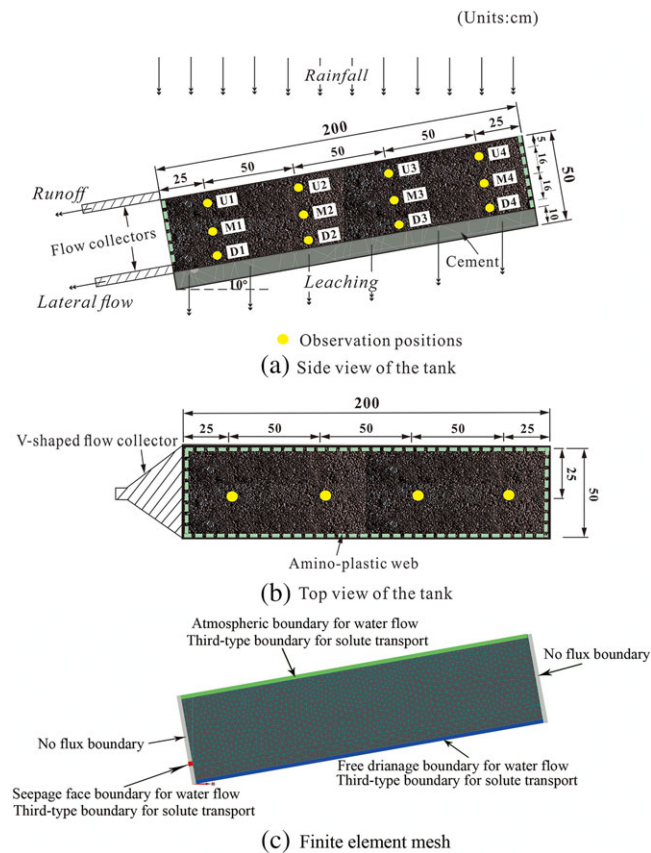


**FIGURE 1** Schematic illustration of the experimental set-up: (a) the side view of the tank, (b) the top view of the tank, and (c) the numerical representation of the tank with the finite element mesh and boundary conditions

under purple soils; 43.5 kg of cement was mixed with 130.4 kg of yellow sand and 36.1 kg of water and stirred well to get a  $2 \text{ g cm}^{-3}$  density. Cement was then paved over the bottom of the tank with 324 uniformly distributed drainage holes of 0.5 cm in diameter. Five litres of water were sprayed at the surface of the cement layer after it hardened. The soils were collected from the top 40-cm layer of the purple sloping farmland in the small Wangjiaqiao watershed ( $110^{\circ}42' \text{ E}$ ,  $31^{\circ}5' \text{ N}$ ), close to the Yichang city in the Zigui County of the Hubei Province, China. The purple sloping land is dominated by a subtropical monsoon climate with intensive rainfall during the summer from June to September. A slope of  $10^{\circ}$ , representing the most common farmland slopes of purple soils, was adjusted by a hydraulic driving device. An amino-plastic web was placed all around the soil tanks to decrease boundary effects between the soil and the steel tank. The air-dried and sifted soil was then backfilled into the steel tank in eight 5-cm layers, and the surface of each layer was roughened to avoid stratification of the interface. The same bulk density as that of the soil collected in the study area ( $1.35 \text{ g cm}^{-3}$ ) was achieved by packing 67.5 kg of soil to each 5-cm-high layer. The particle size distribution of the collected purple soil had the sand ( $>0.05 \text{ mm}$ ), silt (0.002–0.05 mm), and clay contents ( $<0.002 \text{ mm}$ ) of 54.7%, 40.2%, and 5.1%, respectively, and it was classified as loam and Entisol according to the United States Department of Agriculture taxonomy. Additionally, the

nitrogen content of the collected soil was 34.6, 2.86, and 1,107  $\text{mg kg}^{-1}$  for ammonia ( $\text{NH}_4\text{-N}$ ), nitrate ( $\text{NO}_3\text{-N}$ ), and total nitrogen (TN), respectively.

Observations of soil water contents and porewater nitrate concentrations in soils were set up at four positions along the slope at depths of 5, 21, and 37 cm in the upper (U1, U2, U3, and U4), middle (M1, M2, M3, and M4), and bottom (D1, D2, D3, and D4) soil layers (Figure 1). Numbers 1, 2, 3, and 4 represent positions along the direction of the slope 25, 75, 125, and 175 cm away from the bottom side, respectively (Figure 1). Water samples were collected by ceramic cups that were linked using thin plastic pipes with effluent collecting jars. A vacuum pump was used to enhance effluent. Specifically, only the deep and middle layers were equipped with ceramic cups to collect water samples because the suction in the upper layers was not high enough to make ceramic cups collect water effluent. As a result, porewater nitrate concentrations in the upper soil layers were obtained only by model simulations. Additionally, each position was equipped with a moisture sensor based on the frequency domain reflectometry principle with a 5% measurement error.

One day before applying rainfall events, different initial porewater nitrate concentration distributions and similar soil water content ( $0.28 \text{ cm}^3 \text{ cm}^{-3}$ ) distributions were obtained by sprinkling 40 L of water with different amounts of dissolved urea fertilizer. Specifically, 15 g of urea was dissolved in water that was sprinkled uniformly on the soil surface of one tank, achieving a uniform porewater nitrate concentration ( $350 \text{ mg L}^{-1}$ , denoted as a normal [N] initial concentration) distribution along the slope. This scenario was denoted as scenario NNNN. For another soil tank, 7.5 and 5 g of urea was dissolved in two 20-L volumes of water, which were then sprinkled at both ends and in the middle of the sloped soil surface, respectively. As a result, normal and low (about  $180 \text{ mg L}^{-1}$ , denoted as a low [L] initial concentration) concentrations of  $\text{NO}_3\text{-N}$  were distributed at positions 1 and 4, and 2 and 3 (Figure 1), respectively. This scenario was denoted as scenario NLLN. The other three scenarios, that is, LHHH, LNLN, and HHHN, were only simulated using the HYDRUS-2D model, where H represents areas with high initial concentrations (about  $500 \text{ mg L}^{-1}$ , denoted as a high [H] initial concentration).

A stationary artificial rain device was located 9 m above the soil tank. Twelve rainfall events were applied during the laboratory experiment (Figure 2), according to the local climate conditions described above. Specifically, 0.04, 0.1, and  $0.18 \text{ cm min}^{-1}$  were used as light, medium, and heavy rainfall intensities, respectively. All rainfall events lasted 60 min and were applied in 3-day intervals. Three light rainfalls were applied first, followed by three medium rainfalls, and three heavy rainfalls. Finally, the sequence of light, medium, and heavy rainfalls was applied.

Run-off and subsurface flow collectors were installed at the surface and the bottom at the foot of the soil tank (Figure 1), respectively. The subsurface flow collector was welded on the bottom side of the tank next to the interface between the soil and cement layers (Figure 1). Both collectors were protected from rainfall to gather flow only from the soil surface and subsurface.

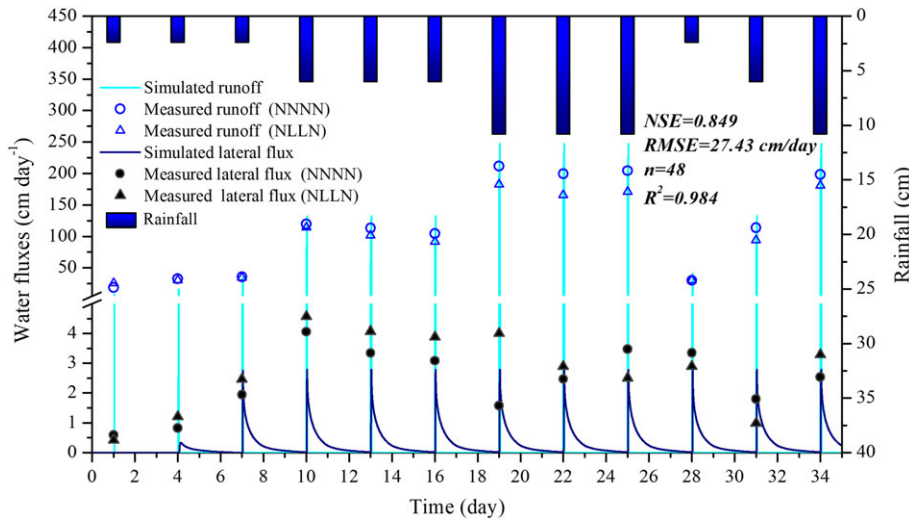


**FIGURE 2** Applied rainfall events, and simulated and observed run-off and lateral fluxes for the NNNN and NLLN nitrate distribution treatments

## 2.1.2 | Measurements and analyses

The run-off was collected into a container with graduation. The flux ( $\text{cm day}^{-1}$ ) was calculated by dividing the discharge volume ( $\text{cm}^3$ ) by the surface area of the tank ( $10,000 \text{ cm}^2$ ) and time (day). Porewater was collected at observation points every 1 hr, and eight samples were collected at each point per event. Porewater  $\text{NO}_3\text{-N}$  concentrations were obtained by averaging concentrations from individual samples. Leaching from the bottom of the soil tank was observed in very small discharge and was not collected. Subsurface flow was collected using measuring cups, and all collected water samples were transferred into clean polyethylene bottles and stored in a refrigerator at  $4^\circ\text{C}$ . The nitrate concentration was determined by a discrete auto analyser (SmartChem 200, Alliance, France) within 48 hr. The lateral nitrate flux ( $\text{mg cm}^{-1} \text{ day}^{-1}$ ) was calculated by dividing the concentration ( $\text{mg cm}^{-3}$ ) by sampling duration (day) and an outflow area ( $\text{cm}^2$ ). The loss (mg) of  $\text{NO}_3\text{-N}$  was calculated by multiplying the total water flux (cm) with the mean nitrate flux ( $\text{mg cm}^{-1}$ ).

## 2.2 | HYDRUS-2D modelling

### 2.2.1 | Modelling set-up

HYDRUS-2D (Šimůnek, van Genuchten & Šejna, 2016) was used in this study to analyse and interpret collected experimental data involving subsurface water flow and  $\text{NO}_3\text{-N}$  transport in sloped soils. The governing equation for uniform water flow is the modified Richards

equation in mixed form describing two-dimensional isothermal uniform Darcian flow of water in a variably saturated rigid porous medium. This equation assumes that the air phase plays an insignificant role in the liquid flow process. The governing equation for solute transport subject to physical and chemical equilibrium is the convection–dispersion equation, which is applied here to simulate nitrate transport. The convection–dispersion equation considers the processes of convection, molecular diffusion, hydrodynamic dispersion, and denitrification of nitrate to nitrogen gas. The two governing equations are numerically solved using the finite element (FE) method. This method requires appropriate spatial and temporal discretization to prevent numerical oscillations and to achieve acceptable mass balance errors (Šimůnek, van Genuchten, & Šejna, 2008). Boundaries of the transport domain involving the purple soil were discretized using 4-cm FEs, whereas 8-cm FEs were used on all other boundaries. In total, 2,509 triangular FEs with 1,219 FE nodes were used to discretize the transport domain for all simulations. Initial, minimum, and maximum time steps of  $10^{-4}$ ,  $10^{-5}$ , and 5 days, respectively, were used in all simulations.

### 2.2.2 | Input parameters

The input parameters required by HYDRUS-2D include soil hydraulic parameters characterizing flow properties of the porous material and solute transport and reaction parameters characterizing nitrate transport and reaction properties (Table 1). The soil hydraulic parameters

**TABLE 1** Optimized values of modelling parameters

Material	Soil type	Water flow parameter					Solute transport and reaction parameters				
		$\theta_r$ ( $\text{cm}^3 \text{ cm}^{-3}$ )	$\theta_s$ ( $\text{cm}^3 \text{ cm}^{-3}$ )	$\alpha$ ( $\text{cm}^{-1}$ )	$n$	$K_s$ ( $\text{cm day}^{-1}$ )	$L$	$D_L$ (cm)	$D_T$ (cm)	$D_w$ ( $\text{cm}^2 \text{ day}^{-1}$ )	$K_{dn}$ ( $\text{day}^{-1}$ )
Purple soil	Loam	0.026	0.413	0.0183	1.5	40	0.5	50	5	1.64	0.015
Cement	Sand shale	0.001	0.069	0.0155	1.5	0.45	0.5	50	5	1.64	0.015

Abbreviations:  $\theta_r$ , the residual water content;  $\theta_s$ , the saturated water content;  $\alpha$  and  $n$ , van Genuchten's shape parameters;  $K_s$ , the saturated hydraulic conductivity;  $L$ , the pore connectivity parameter;  $D_L$ , the longitudinal dispersivity;  $D_T$ , the transverse dispersivity;  $D_w$ , the molecular diffusion coefficient in free water;  $K_{dn}$ , the denitrification rate.

( $\theta_r$ ,  $\theta_s$ ,  $\alpha$ ,  $n$ , and  $K_s$ : the residual and saturated water contents, two shape parameters, and the saturated hydraulic conductivity, respectively) for the van Genuchten (1980) functions and the statistical pore-size distribution model of Mualem (1976) were initially estimated for the purple soil using neural networks from textural information (Schaap, Leij, & van Genuchten, 1998). The hydraulic parameters for the cement layer were obtained from Schneider, Baumgartl, Doley, and Mulligan (2010). The pore connectivity parameter  $L$  was assumed to be 0.5 (Mualem, 1976). No hysteresis was considered in all simulations. For the nitrate transport, the longitudinal dispersivity,  $D_L$  (20 cm, the same value was considered for both soil and cement), was initially set equal to one tenth of the travel distance; the transverse dispersivity,  $D_T$  (2 cm), was assumed to be one tenth of  $D_L$ ; and the molecular diffusion coefficient in free water,  $D_w$ , and the denitrification rate,  $K_{dn}$ , for  $\text{NO}_3\text{-N}$  were  $1.64 \text{ cm}^2 \text{ day}^{-1}$  and  $0.015 \text{ day}^{-1}$ , respectively (Li et al., 2015).

### 2.2.3 | Initial and boundary conditions

The initial water content was assumed to be distributed uniformly in the soil tank after water infiltration at the soil surface. The average initial water content of the soil ( $0.28 \text{ cm}^3 \text{ cm}^{-3}$ ) was obtained by soil moisture sensors. The initial water content in the cement representing the bedrock was set equal to  $0.05 \text{ cm}^3 \text{ cm}^{-3}$ , that is, the volume of water applied to the cement divided by the volume of the cement. The soil tank was divided into four sections centred around positions 1, 2, 3, and 4 (25, 75, 125, and 175 cm from the slope bottom). The initial nitrate content was assumed to be distributed uniformly in each section (Table 2, N: normal; H: high; L: low). Timing of rainfalls and their intensity were set as shown in Figure 2 according to actual applied rainfall events. Evaporation and transpiration fluxes were not considered in simulations. An atmospheric boundary condition was assigned to the soil surface boundary, and time-dependent precipitation events were specified as discussed above. Actual surface flux and run-off were calculated internally by the program. Considering the experimental set-up, the bottom boundary of the soil tank was set as a free drainage boundary condition, and a seepage face boundary condition (1 cm long) was assigned on the left side of the soil tank above the interface between the soil and the cement layer. These boundary conditions represent vertical leaching and saturated lateral flow, respectively. A third-type boundary condition (a Cauchy boundary condition) for solute transport was assigned to all inflow and outflow

boundaries. The other water flow and solute transport boundaries were set as no flux boundary conditions. Figure 1c shows boundary conditions applied to the transport domain.

## 2.3 | Model evaluation

Simulated data for surface run-off and porewater nitrate concentrations were compared with corresponding observed data from the laboratory experiments. One set of soil tank experimental data (the NNNN treatment in Table 2) was used to calibrate the input model parameters, and another set of observed data (the NLLN treatment in Table 2) was used to validate the calibrated model. Three statistical measures were used to evaluate the model performance: the Nash–Sutcliffe model efficiency coefficient ( $NSE$ ), the root mean square error ( $RMSE$ ), and the coefficient of determination ( $R^2$ ) at  $p = .05$ .  $NSE$  and  $RMSE$  were calculated as

$$NSE = 1 - \frac{\sum_1^n (M_i - S_i)^2}{\sum_1^n (M_i - \bar{M})^2}, \quad (1)$$

$$RMSE = \sqrt{\frac{1}{n} \sum_1^n (S_i - M_i)^2}, \quad (2)$$

where  $M_i$  and  $S_i$  are measured and simulated values, respectively, and  $n$  is the number of experimental data points. The  $R^2$  was calculated internally by Excel (Microsoft Corp., WA, USA) using the trend line fitting. Optimal values for  $NSE$ ,  $RMSE$ , and  $R^2$  are 1, 0, and 1, respectively. Specifically, satisfactory and good model performances are obtained when  $NSE$  is larger than 0.5 and 0.65, respectively (Wang et al., 2018).

## 3 | RESULTS

### 3.1 | Model calibration and validation

Measured run-off, subsurface lateral fluxes, and soil water contents at observation positions were used to calibrate and validate the soil hydraulic parameters. Simulated run-off fluxes for the NNNN and NLLN treatments were identical because the same initial and boundary conditions were used for both treatments. A good agreement between observed and simulated water fluxes was obtained (Figure 2,  $NSE = 0.849$ ,  $RMSE = 27.43 \text{ cm day}^{-1}$ ,  $n = 48$ ,  $R^2 = 0.984$ ). A similarly

**TABLE 2** Initial nitrate concentration distributions along the slope for various treatments

Nitrate distributions	Sections	Treatments				
		NNNN	NLLN	LHHL	LNLN	HNHN
Initial nitrate concentrations ( $\text{mg L}^{-1}$ )	1	350	350	180	180	500
	2	350	180	500	350	350
	3	350	180	500	180	500
	4	350	350	180	350	350

Note. Sections 1, 2, 3, and 4 are centred around positions 25, 75, 125, and 175 cm from the slope foot along the slope direction, respectively.

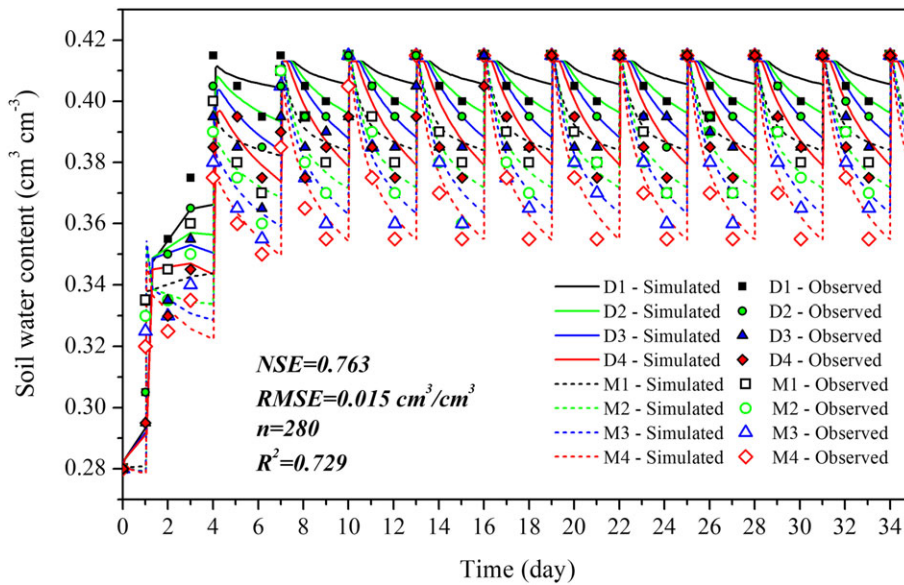


**FIGURE 3** Simulated and observed soil water contents at positions M1, M2, M3, M4, D1, D2, D3, and D4

good agreement was also obtained between observed and simulated water contents at the observed positions (Figure 3,  $NSE = 0.763$ ,  $RMSE = 0.015 \text{ cm}^3 \text{ cm}^{-3}$ ,  $n = 280$ ,  $R^2 = 0.729$ ). Both water fluxes and water contents showed similar dynamics between simulated and observed data.

Porewater  $\text{NO}_3\text{-N}$  concentrations observed in subsurface soil layers (M1, M2, M3, M4, D1, D2, D3, and D4) and lateral  $\text{NO}_3\text{-N}$  fluxes for the uniform normal fertilizer distribution (the NNNN treatment) were used to calibrate solute transport. Calibrated values of the longitudinal ( $D_L$ ) and transverse ( $D_T$ ) dispersivities were 50 and 5 cm ( $D_T = D_L/10$ ), respectively, for both purple soil and cement layers. In comparison, the molecular diffusion coefficient in free water ( $D_w$ ) and the denitrification rate ( $K_{dn}$ ) were not calibrated as the results were relatively insensitive to their values.  $NSE$  and  $RMSE$  of porewater nitrate dynamics for the calibrated model (for the NNNN treatment) are 0.833 and  $39.2 \text{ mg L}^{-1}$  ( $n = 96$ ,  $R^2 = 0.894$ , Figure 4a), respectively.  $NSE$  and  $RMSE$  of lateral nitrate fluxes for the calibrated model are 0.902 and  $6.75 \text{ mg cm}^{-1} \text{ day}^{-1}$  ( $n = 156$ ,  $R^2 = 0.947$ , Figure 5), respectively. These  $NSE$  ( $>0.75$ ) showed very good model performance (Wang et al., 2018) despite a relatively large  $RMSE$  (about one tenth of  $C_0$ ). The largest differences between measured and simulated nitrate concentrations were found at D1 (Figure 4). Contrary to experimental data that showed relatively large spatial differences in nitrate concentrations at the same depth after the third rainfall, simulated results showed much less spatial variance in nitrate dynamics (Figure 4a). This can potentially be explained by the fact that observed soil water contents at the slope foot decreased faster than simulated values and that observed soil water contents displayed hysteretic behaviour (Figure 3). As a result, observed nitrate dynamics displayed the largest decrease at D1 and the smallest at D4 (Figure 4a).

Concentrations observed in another soil tank with a non-uniform initial nitrate distribution along the slope (the NLLN treatment) were then used to validate the model for calibrated solute transport and reaction parameters. Good model performance, although less good

than during calibration, was also obtained during model validation with  $NSE$  of 0.744 and  $RMSE$  of  $35.6 \text{ mg L}^{-1}$  ( $n = 96$ ,  $R^2 = 0.774$ , Figure 4b) for porewater nitrate dynamics. Differences between simulated and observed nitrate concentrations at position D1 were the main cause of lower simulation accuracy during validation than during calibration. It can be seen that simulated nitrate concentrations were smaller than those observed at D1 for the NLLN treatment (Figure 4b). These discrepancies between experimental and modelling results may be caused by the combined effects of water flow and nitrate transport. In contrast, simulated lateral nitrate fluxes showed a very good modelling performance with  $NSE$  of 0.881 and  $RMSE$  of  $7.13 \text{ mg cm}^{-1} \text{ day}^{-1}$  ( $n = 156$ ,  $R^2 = 0.977$ , Figure 5).

Although HYDRUS-2D simulated decreasing trends in nitrate concentrations and fluxes that were consistent with the experimental results, it could not fully capture the entire variability in the observed data, as reflected by the  $RMSE$ s between observed and simulated data, which were on the order of 10% of  $C_0$ . Despite these discrepancies, an overall relatively good description of observed surface runoff, subsurface fluxes, water contents, and nitrate concentrations during both calibration and validation indicates that the HYDRUS-2D model can be used with calibrated parameters (Table 1) to analyse other experimental treatments, as well as other potential scenarios.

Figure 4 shows a similarly decreasing trend in porewater nitrate concentrations at all observation points. Porewater nitrate concentrations at points subjected to normal fertilizer application displayed a sharply decreasing, exponential trend during the first 5 days of the experiment. Nitrate concentrations tended to be more stable in the range between 50 and  $100 \text{ mg L}^{-1}$  during later stages of the experiment. Discrepancies between simulated and observed nitrate dynamics can be partly explained by differences between simulated and actual soil water contents (Figure 3). Figure 4 shows that simulated nitrate concentrations registered significant, sharp declines immediately after rainfall, especially during early stages of the experiment.

**FIGURE 4** Simulated and observed porewater NO<sub>3</sub>-N concentrations at D1, D2, D3, and D4 for the (a) NNNN and (b) NLLN nitrate distribution treatments. Results displayed in (a) were used for model calibration and those displayed in (b) for model validation

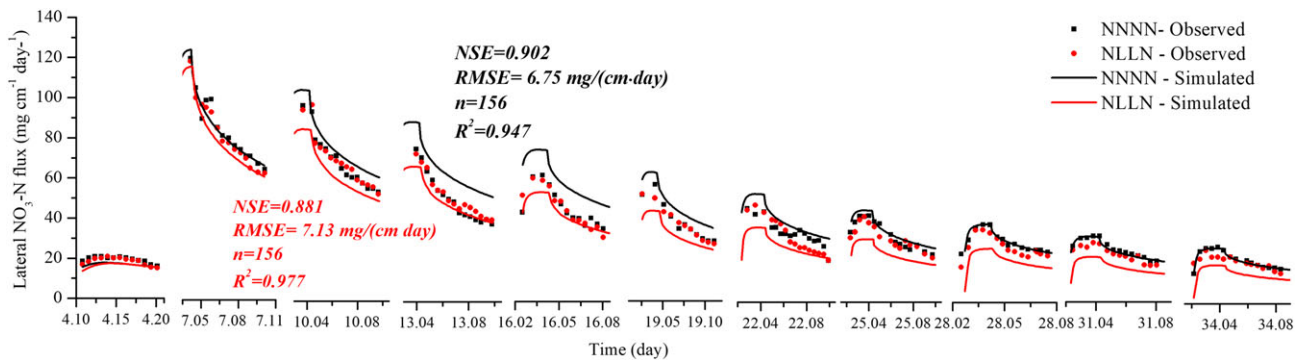
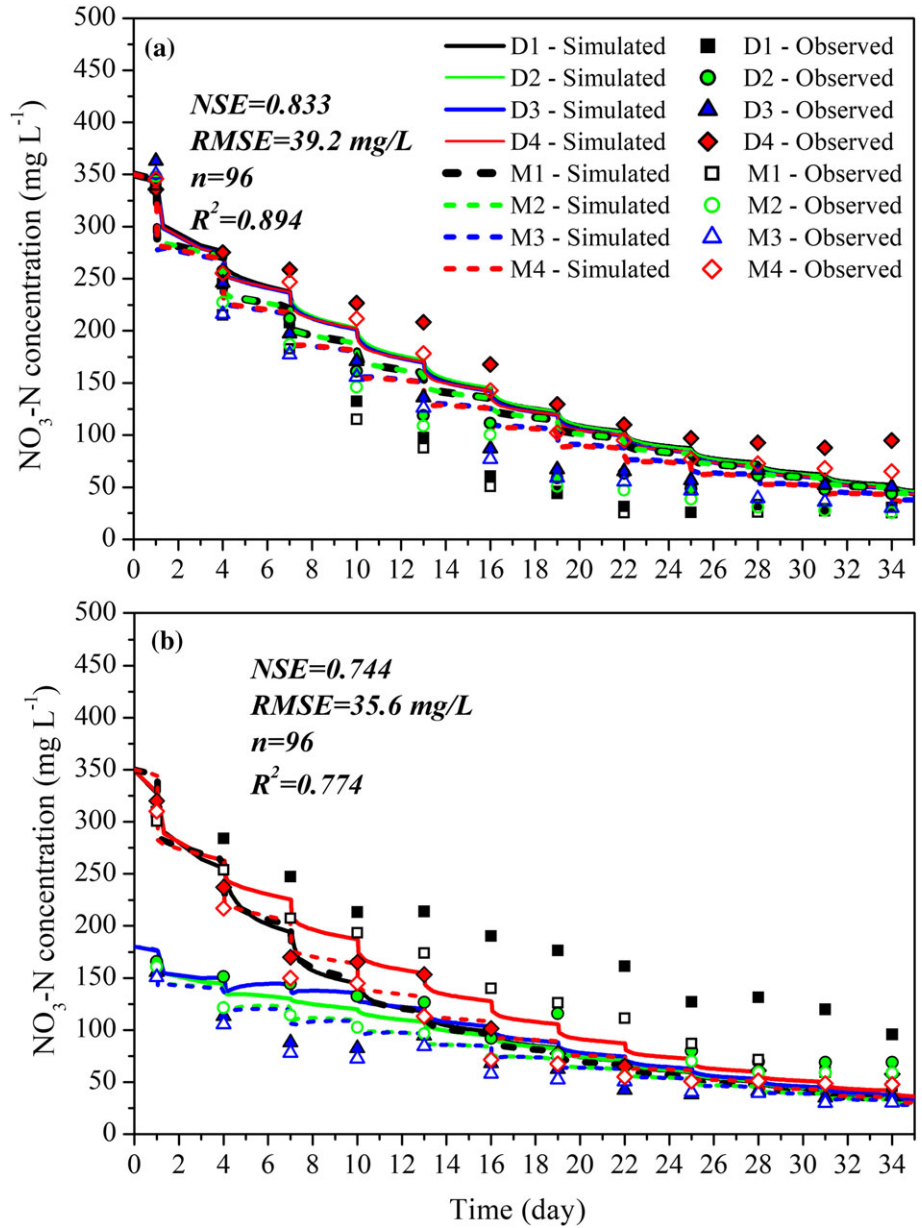


**FIGURE 5** Simulated and observed lateral NO<sub>3</sub>-N fluxes for the NNNN and NLLN nitrate distribution treatments. Results displayed in black were used for model calibration and those displayed in red for model validation



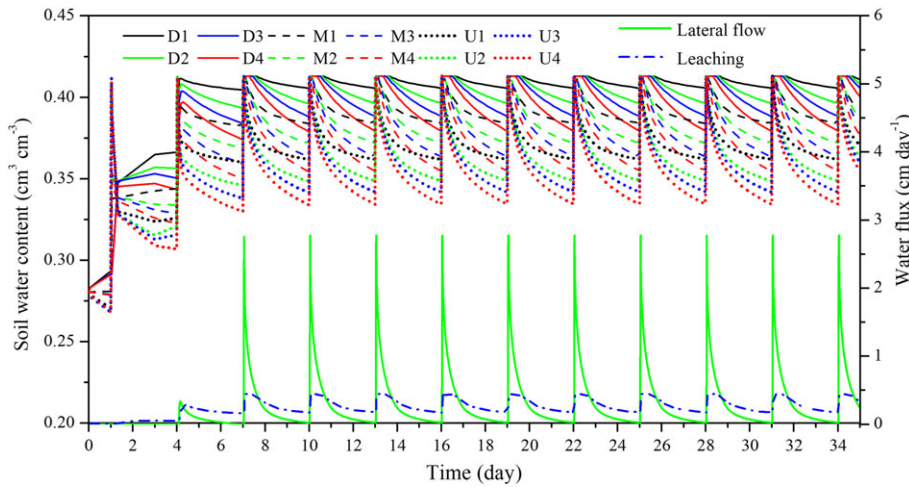


**FIGURE 6** Simulated soil water contents at 12 observation points and subsurface lateral and vertical leaching water fluxes

### 3.2 | Water fluxes

Figures 2 and 6 show that water losses due to run-off, subsurface lateral flow, and vertical leaching occurred simultaneously, even if at different levels, with run-off fluxes significantly larger than subsurface and leaching fluxes. Specifically, rainfall played a greater positive role on run-off, whereas soil water contents had stronger positive effects on subsurface flow. During the first three low intensity rainfall events ( $0.04 \text{ cm min}^{-1}$ ), run-off increased from  $7.9$  to  $35.8 \text{ cm day}^{-1}$ , and soil water contents increased from the initial value to the saturated water content. Subsequent rainfall events (with moderate and high intensities) produced run-off, which was proportional to the rainfall intensity, contrary to maximum subsurface lateral flow and vertical leaching, which were independent of the rainfall intensity. Numerical simulations indicate that rainfall of  $6$  and  $10.8 \text{ cm}$  produced the largest run-off fluxes of  $132.2$  and  $247.5 \text{ cm day}^{-1}$  (Figure 2), respectively, compared with the maximum lateral flow of  $2.8 \text{ cm day}^{-1}$  and the maximum leaching of  $0.4 \text{ cm day}^{-1}$  (Figure 6). However, both processes of lateral flow and leaching lasted much longer (Figure 6) than run-off (Figure 2) for each rainfall. The major water loss from sloped soils was thus attributed to surface run-off, followed by lateral flow, and vertical leaching. Lateral flow occurred only when the soil became saturated at the interface between the soil and bedrock layers. Vertical leaching was a continuous process, although at a relatively low flow rate. Leaching flow towards deep groundwater occurred at rates from  $0.008$  to  $0.4 \text{ cm day}^{-1}$  before the soil reached full saturation, when its maximum values occurred. Soil water contents displayed similar dynamics as lateral flow and vertical leaching, with corresponding maximum and minimum values occurring at the same time (Figure 6).

### 3.3 | $\text{NO}_3\text{-N}$ transfer in response to different initial distributions

Figure 7 shows simulated temporal changes in relative nitrate concentrations at 12 different locations of the sloped soils subjected to five various initial spatial distributions of porewater nitrate concentrations. Nitrate concentrations showed the smallest variations

between positions in the NNNN treatment, during which initial concentrations were the same everywhere. The largest variations were obtained when two different initial concentrations were used in the LHHL treatment. Overall,  $\text{NO}_3\text{-N}$  concentrations displayed exponential declining trends and almost instantaneous response to rainfall events. Simulated average residual  $\text{NO}_3\text{-N}$  concentrations for all initial nitrate concentration distributions tended to be about  $50 \text{ mg L}^{-1}$ . Relative residual  $\text{NO}_3\text{-N}$  concentrations ( $C/C_0$ ) were larger in locations with lower initial concentrations ( $C_0$ ; Figure 7). Larger differences between relative decreases in nitrate concentrations at 12 observed positions occurred for treatments with non-uniform initial nitrate distributions (Figure 7b–e). In all treatments, nitrate concentration decreases were larger in the upper soil layers. However, the smallest differences between nitrate concentrations in three soil layers were at the foot of the slope (D1, M1, and U1) under the NNNN, NLLN, and HNHN treatments (Figure 7a,b,e), whereas the largest differences were under the LHHL and LNLN treatments (Figure 7c,d). Non-uniform initial nitrate distributions contributed to larger differences between four locations along the slope in the deeper soil layers.

$\text{NO}_3\text{-N}$  concentrations on the fifth day are used below to analyse the decreasing trend in response to different initial nitrate spatial distributions because nitrate concentrations on this day were in the middle stage of sharp declines (Figure 7). Relative  $\text{NO}_3\text{-N}$  concentrations ( $C/C_0$ ) with respect to the corresponding initial concentration ( $C_0$ ) were about  $0.56$  at U2, U3, and U4 positions,  $0.65$  at U1, M1, M2, M3, and M4 positions, and  $0.7$  at D1, D2, D3, and D4 positions in the NNNN treatment (Figure 7a). Non-uniform initial nitrate distributions produced different decreasing trends. In the NLLN treatment, values of  $C/C_0$  were about  $0.55$  at U1 and U4,  $0.6$  at D1, M1, and M4, and  $0.68$  at D4 and decreased faster in the initially normal domain (Figure 7b) than those in the uniform distribution treatment. In the same soil layer, corresponding values were larger and decreased slower in the initially low domain of the NLLN treatment. In the LHHL treatment, values of  $C/C_0$  were about  $0.53$  at U2 and U3,  $0.6$  at M2 and M3,  $0.65$  at D3, and  $0.69$  at D2 with high initial nitrate concentrations (Figure 7c). In the LNLN treatment, values of  $C/C_0$  were about

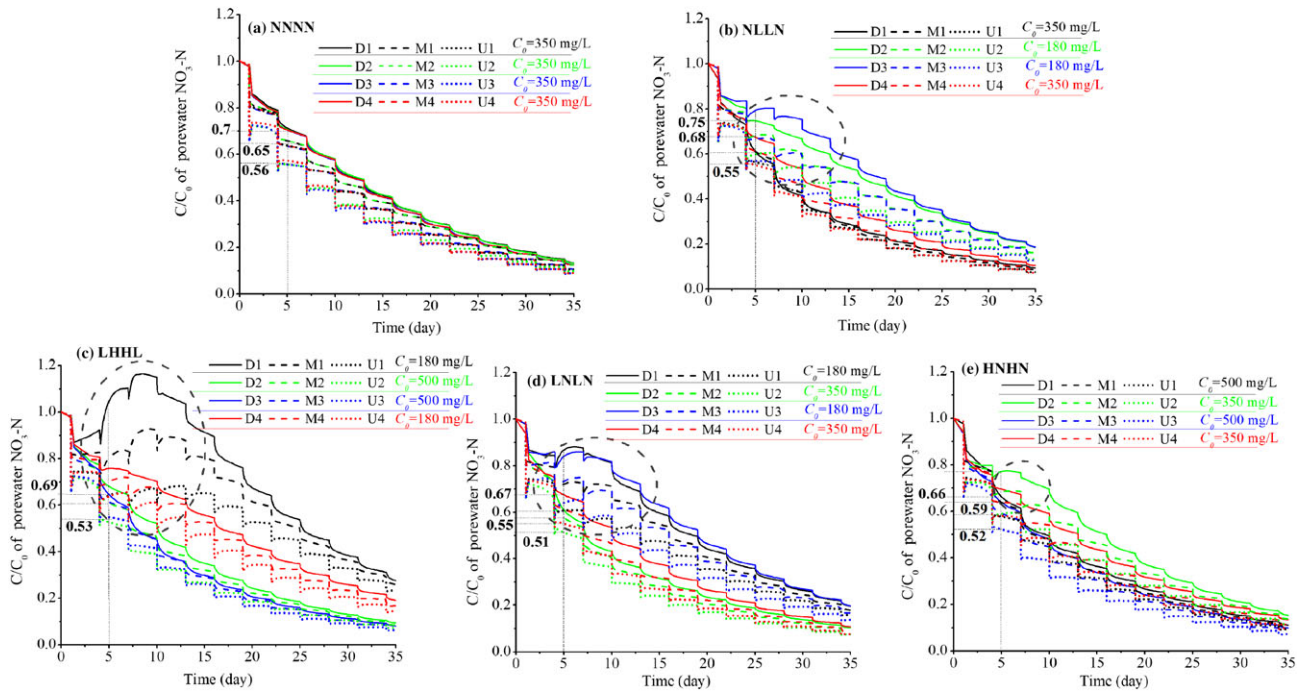


**FIGURE 7** Simulated relative  $\text{NO}_3\text{-N}$  concentrations ( $C/C_0$ ) at 12 observation positions for five different initial nitrate distribution treatments: (a) NNNN, (b) NLLN, (c) LHHL, (d) LNLN, and (e) HNHN.  $C_0$  is the initial concentration

0.51 at U2, 0.55 at U4, 0.58 at M2, 0.6 at D2 and M4, and 0.67 at D4 with normal initial nitrate concentrations (Figure 7d), which is similar to the NLLN treatment. In the HNHN treatment, values of  $C/C_0$  were 0.77 and 0.70 at D2 and D4, respectively, with high initial nitrate concentrations and 0.66 and 0.64 at D1 and D3, respectively, with low initial nitrate concentrations (Figure 7e). These trends indicate that non-uniform initial distributions contributed to slower and faster nitrate concentration decreases in areas with lower and higher initial nitrate concentrations, respectively, due to the lateral transfer of nitrate between the two domains to compensate for lower initial nitrate contents.

Regions with lower initial concentrations in the non-uniform distribution treatments registered significant increases in relative concentrations during early stages of the experiment as indicated by grey dashed-line circles in Figure 7. Regions with low initial nitrate concentrations ( $180 \text{ mg L}^{-1}$ ) registered the largest increases due to the compensation from regions with high initial nitrate concentrations (Figure 7c). Increases in nitrate concentrations correlated positively with the soil depth. These increases tended to be prolonged with small increments in the upper soil layers. Also, the compensation from regions with normal initial concentrations was larger in the LNLN treatment than in the NLLN treatment, which indicates that the low concentration region at the foot of the slope obtained higher  $\text{NO}_3\text{-N}$  compensation. Relative concentrations in regions with higher initial concentrations always decreased faster than in other regions. The compensation becomes smaller when the concentration difference between neighbouring regions decreases. However, all  $\text{NO}_3\text{-N}$  concentrations tended to decline with time after rainfall was initiated.

### 3.4 | $\text{NO}_3\text{-N}$ fluxes and losses due to subsurface flow and vertical leaching

Figure 5 shows comparisons between observed and simulated lateral  $\text{NO}_3\text{-N}$  fluxes. Although both simulated and observed fluxes displayed similar dynamics, differences between observed lateral  $\text{NO}_3\text{-N}$  fluxes for two different initial nitrate distributions were smaller than those simulated. Differences in measured lateral  $\text{NO}_3\text{-N}$  fluxes between the two treatments can be explained by the observed spatial variability in porewater nitrate concentrations (Figure 4). However, in general, observed  $\text{NO}_3\text{-N}$  fluxes for the NNNN treatment were larger than those for the NLLN treatment.

Figure 8 shows simulated subsurface lateral and vertical leaching  $\text{NO}_3\text{-N}$  fluxes for five different initial  $\text{NO}_3\text{-N}$  distribution treatments.  $\text{NO}_3\text{-N}$  fluxes displayed gradually decreasing peak values during subsequent rainfall events except for the first two low intensity rainfalls.  $\text{NO}_3\text{-N}$  fluxes reached maximum peak values on the seventh day (after three low intensity rainfalls) when for the first time water fluxes reached their maximum values. After then, peak values tended to decrease similarly as porewater nitrate concentrations in the soil. However, lateral nitrate fluxes under the LHHL treatment peaked on the 10th day and after that tended to be equal to the peak values for the NNNN and HNHN treatments. Overall,  $\text{NO}_3\text{-N}$  fluxes correlated positively with corresponding water fluxes, as shown in Figure 6. As a result, peak values of  $\text{NO}_3\text{-N}$  lateral fluxes were much larger than corresponding  $\text{NO}_3\text{-N}$  leaching fluxes, both getting smaller after each rainfall event. After each rainfall, leaching nitrate fluxes decreased slower than lateral nitrate fluxes. Between rainfall events, vertical nitrate leaching continued (Figure 8b), whereas lateral nitrate fluxes

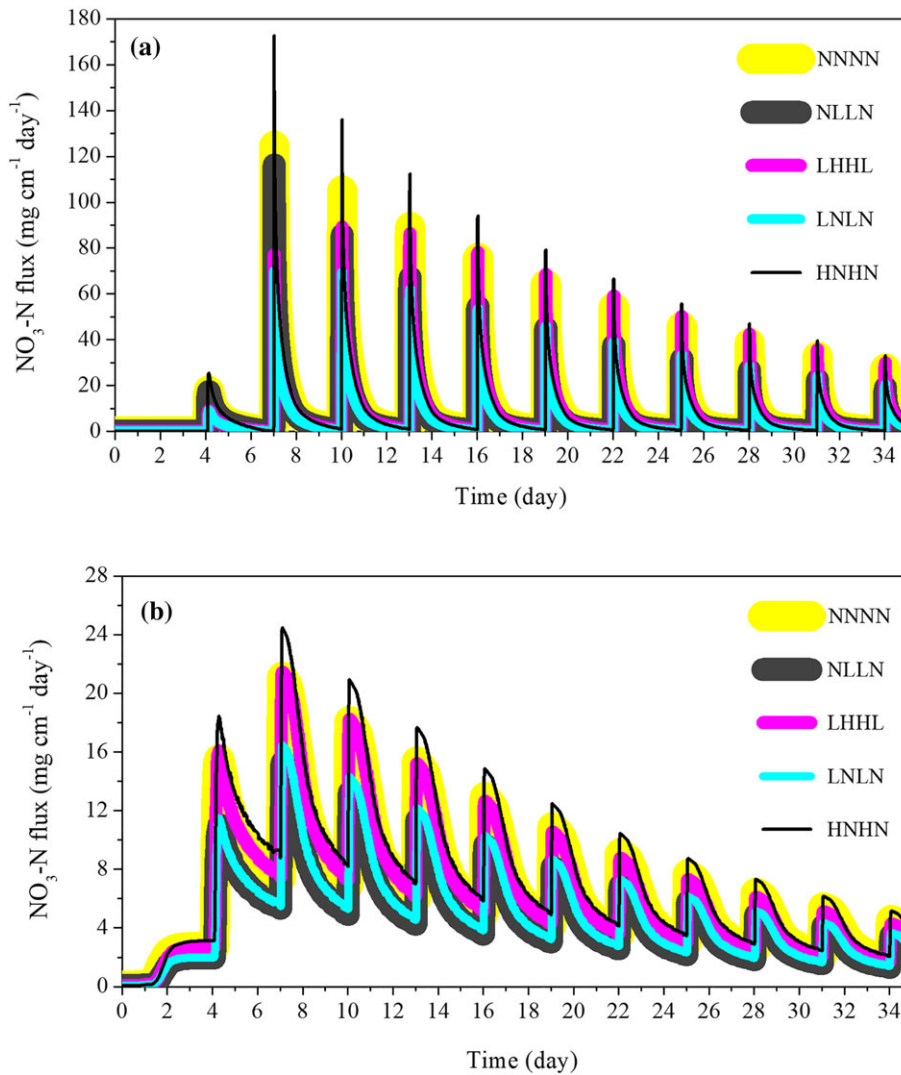


**FIGURE 8** Simulated  $\text{NO}_3\text{-N}$  lateral flow (a) and vertical leaching (b) fluxes for various initial nitrate distribution treatments

tended to stop (Figure 8a). Vertical leaching  $\text{NO}_3\text{-N}$  fluxes were more persistent than lateral nitrate fluxes between two rainfall events (Figure 8), similarly as lateral and leaching water fluxes (Figure 6). Average  $\text{NO}_3\text{-N}$  lateral fluxes ranged from 9.6 to 17.5  $\text{mg cm}^{-1} \text{day}^{-1}$ . Average  $\text{NO}_3\text{-N}$  leaching fluxes ranged from 5.6 to 8.8  $\text{mg cm}^{-1} \text{day}^{-1}$ . In other words,  $\text{NO}_3\text{-N}$  lateral fluxes were about twice as large as  $\text{NO}_3\text{-N}$  leaching fluxes for the same initial nitrate distribution treatments (Figure 9). However, total  $\text{NO}_3\text{-N}$  fluxes due to vertical leaching (238, 174, 241, 183, and 278  $\text{mg cm}^{-1}$  for the NNNN, NLLN, LHHL, LNLN, and HNHN treatments, respectively) were almost the same as those due to subsurface lateral flow (216, 162, 210, 150, and 272  $\text{mg cm}^{-1}$  for the NNNN, NLLN, LHHL, LNLN, and HNHN treatments, respectively; Figure 10).

In response to different initial nitrate distributions,  $\text{NO}_3\text{-N}$  lateral fluxes displayed larger differences than  $\text{NO}_3\text{-N}$  leaching fluxes. Specifically, maximum subsurface lateral  $\text{NO}_3\text{-N}$  fluxes during the second light rainfall were 25.3 and 9.2  $\text{mg cm}^{-1} \text{day}^{-1}$  for the HNHN and LNLN treatments, respectively, whereas maximum leaching  $\text{NO}_3\text{-N}$  fluxes were 18.4 and 11.4  $\text{mg cm}^{-1} \text{day}^{-1}$ , respectively. On the other hand, maximum subsurface lateral  $\text{NO}_3\text{-N}$  fluxes were 172.7 and

70.0  $\text{mg cm}^{-1} \text{day}^{-1}$  for the HNHN and LNLN treatments, respectively, whereas maximum leaching  $\text{NO}_3\text{-N}$  fluxes were 24.5 and 16.5  $\text{mg cm}^{-1} \text{day}^{-1}$ , respectively. Largest (2,766  $\text{mg}$  for lateral flow and

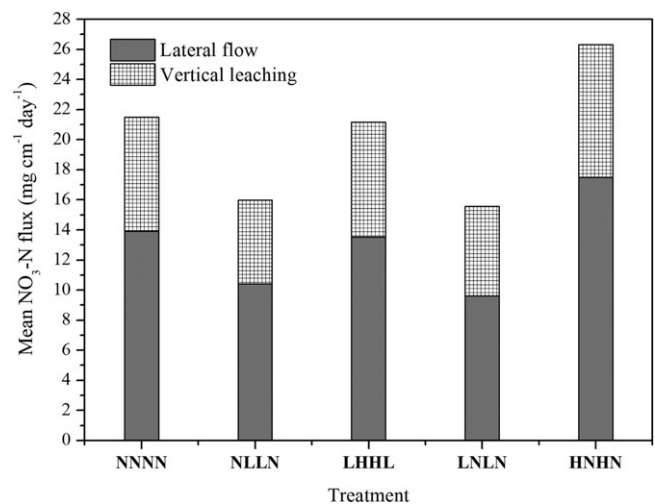


**FIGURE 9** Mean  $\text{NO}_3\text{-N}$  lateral flow and vertical leaching fluxes for various initial nitrate distribution treatments

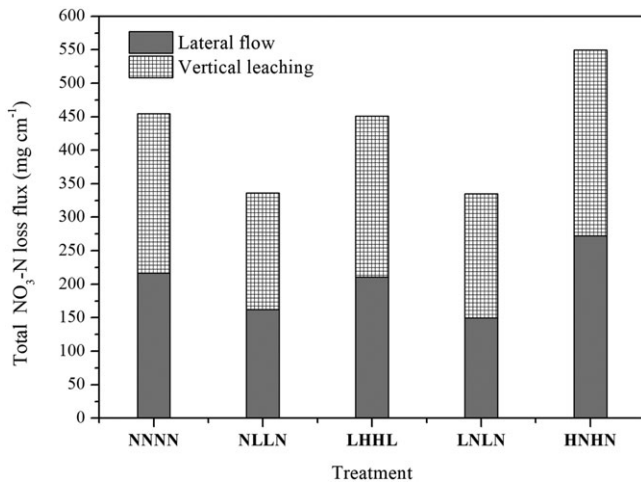


**FIGURE 10** Total NO<sub>3</sub>-N losses due to lateral flow and vertical leaching for various initial nitrate distribution treatments

1,304 mg for leaching) NO<sub>3</sub>-N losses were obtained for the HNHN treatment. Smallest lateral (1,522 mg) and leaching (823 mg) NO<sub>3</sub>-N losses occurred under the LNLN and NLLN initial nitrate distributions. It is noteworthy that mean and total nitrate losses were almost the same for the NLLN and LNLN treatments (Figures 9 and 10), which had the same initial amount of fertilizer in the tank. The minimum NO<sub>3</sub>-N loss occurred for the treatment with the smallest amount of applied fertilizer.

## 4 | DISCUSSION

### 4.1 | Effects of different factors on NO<sub>3</sub>-N transport and losses

#### 4.1.1 | Soil water

Previous studies have highlighted the effects of rainfall intensity and duration on subsurface NO<sub>3</sub>-N transport and losses from purple sloped soils (Jia et al., 2007; Xie, Zhang, Zhang, & Chen, 2018). Rainfalls directly affect soil water contents as a result of infiltration. Nitrate is easily soluble in water and very mobile (Hamoudi & Belkacemi, 2013; Kanthle, Lenka, Lenka, & Tedia, 2016). In this study, all peak values of water and NO<sub>3</sub>-N fluxes displayed simultaneous declines after saturated stages (Figures 6 and 8), indicating that soil water losses accompanied NO<sub>3</sub>-N losses. Similarly, Baram et al. (2016) reported that mobile water was responsible for most of the nitrate transport in the deep vadose zone. Observed and simulated water contents in the middle and deep soil layers displayed the same dynamics (Figure 3). However, although simulated soil water contents at all positions tended to consistently reach full saturation after rainfalls, observed soil water contents displayed a hysteretic behaviour (not considered in simulations) at higher positions of the tank. Hence, observed nitrate concentrations displayed spatial variations, whereas simulated porewater NO<sub>3</sub>-N concentrations were more consistent along the slope (Figure 4a). Figures 6 and 7 show that simulated nitrate concentrations at observation points decreased sharply after

rainfalls when soil water contents increased to saturation. Sharp NO<sub>3</sub>-N declines occurred especially during the first three rainfall events when soil water contents gradually increased towards saturation. Larger decreases in nitrate concentrations in the upper soil layers were related to larger rainfall events and faster increases in the soil water content towards saturation. Additionally, faster decreases of observed soil water content at the slope foot caused larger declines in nitrate concentrations compared with simulated data. When the numerical simulations were extended without applying additional rainfall, porewater NO<sub>3</sub>-N concentrations remained more or less constant, whereas soil water contents gradually decreased (due to vertical leaching). This indicates that soil water affected nitrate transport by means of elution as a response to rainfall.

#### 4.1.2 | Initial NO<sub>3</sub>-N distributions

Different initial nitrate distributions were the result of different amounts of nitrogen fertilizer applied to soils (Li, Zhang, & Rao, 2004; Wang et al., 2010; Xu, Niu, Xu, & Wang, 2013). Xu et al. (2013) reported that nitrate concentrations in soils and leaching were related to initial conditions according to observed and simulated data. We operated under the assumption that the initial nitrate distribution was uniform in the vertical direction. Simulated different initial nitrate distributions caused different declines in nitrate concentrations, as shown in Figure 7. Although there was least distinct spatial variation in NO<sub>3</sub>-N transport in sloped soils in the NNNN treatment, there were significant differences in soils with non-uniform initial nitrate distributions. Nitrate concentrations increased at an early stage of the experiments at locations with lower initial nitrate concentrations in non-uniform treatments, especially in the deep soil layers. Also, nitrate concentrations (both observed and simulated) declined slower at these locations compared with locations with higher initial nitrate concentrations (Figures 4b and 7). It can be seen that nitrate redistributed from locations with higher initial concentrations to locations with lower initial concentrations. More nitrate was then eluted from tank sections with higher initial nitrate contents due to subsurface lateral flow and vertical leaching, producing more pollutions to watershed and groundwater.

The first two peaks of lateral NO<sub>3</sub>-N fluxes (Figure 8) decreased in the following order for different treatments: HNHN > NNNN > NLLN > LHHL > LNLN. A different order (HNHN > NNNN > LHHL > LNLN > NLLN) was found for peak values of vertical NO<sub>3</sub>-N leaching fluxes. Higher initial nitrate concentrations at the slope foot produced larger lateral NO<sub>3</sub>-N fluxes during each rainfall event, whereas vertical nitrate leaching fluxes were positively correlated with total amounts of nitrate applied. Essentially, both NO<sub>3</sub>-N losses due to lateral flow and vertical leaching depended on porewater nitrate concentrations in the vicinity of the outflow boundary (the seepage face boundary for lateral flow and the free drainage boundary for vertical leaching) where losses occur. Rapid declines of nitrate concentrations in locations with higher initial concentrations caused different nitrate distributions during subsequent rainfall events. As a result, peak values of lateral NO<sub>3</sub>-N fluxes decreased in a different order for the NLLN and

LHHL treatments (LHHL > NLLN). Also, differences in peak values among all treatments decreased, especially between the NLLN and LNLN treatments with the same initial total nitrate contents. Figures 9 and 10 show that the mean and total  $\text{NO}_3\text{-N}$  fluxes displayed the same descending patterns for the five treatments (HNHN > NNNN > LHHL > NLLN > LNLN for lateral flow and HNHN > NNNN > LHHL > LNLN > NLLN for vertical leaching). Differences between the NLLN and LNLN treatments were negligible, similarly as between the NNNN and LHHL treatments (with similar initial nitrate contents). Overall, treatments with higher nitrogen applications caused higher subsurface nitrate losses. Wang et al. (2018) reported that soil nitrate leaching increased rapidly with increasing nitrogen application rates. There is thus a positive correlation between nitrate concentrations at the interface where losses occur, nitrate applications, and subsurface nitrate losses.

The  $\text{NO}_3\text{-N}$  transport in sloped soils with a uniform initial nitrate distribution showed the least spatial variability. However, spatial variabilities were significant for initially non-uniform distributions. The spatial variability along the slope can be attributed to convection with soil water and dispersion due to concentration gradients. Larger decreases in nitrate concentrations due to water dilution in the upper soil layers were found in this study. Similarly, Li and Liu (2011) found that nitrate concentrations increased with soil depth by applying nitrate solution in uniform soils. At first, non-uniform nitrate distributions produced faster declines in regions with higher initial nitrate concentrations and slower decreases in regions with lower initial nitrate concentrations. The effects of non-uniform distributions on  $\text{NO}_3\text{-N}$  transfer were more pronounced at the deep soil layer (Figure 7). We suggest that non-uniform applications should be taken into account in fertilizer management on sloped soils. Specifically, smaller amounts of nitrate fertilizers should be applied near the slope foot and larger amounts upslope in order to reduce nitrate losses and increase downslope fertility.

## 4.2 | Differences in $\text{NO}_3\text{-N}$ losses due to lateral flow and vertical leaching

Saturated subsurface flow was collected at the foot side of the slope. This lateral flow occurred along an inclined bedrock that had a significantly lower permeability than the overlaying soil (Allaire, Roulier, & Cessna, 2009; Dusek, Vogel, Dohnal, & Gerke, 2012; Xie et al., 2018). In the HYDRUS-2D model, water leaves the saturated part of the flow domain laterally through a seepage face. Although there are short-duration flux peaks (Figure 6) corresponding with rainfalls, lateral flow through this boundary stops when the soil becomes unsaturated (i.e., the pressure head becomes negative). In contrast, vertical leaching at the bottom of the bedrock was simulated using a free drainage boundary condition, which resulted in a continuous bottom flux equal to the unsaturated hydraulic conductivity corresponding to the pressure head at the domain bottom. The leaching flux is thus incessant, increasing visibly (but much less than for lateral flow) after intensive rainfalls (Figure 6). As a result, total lateral flow (9.3 cm) and vertical leaching (8.7 cm) during

the experiment were almost the same. Similarly, total nitrate fluxes due to lateral flow were almost the same as those due to vertical leaching (Figure 10). This occurred even though peak values of water and nitrate fluxes for lateral flow ( $2.8 \text{ cm day}^{-1}$  and  $173 \text{ mg cm}^{-1} \text{ day}^{-1}$ , respectively) were much larger than those for vertical leaching ( $0.44 \text{ cm day}^{-1}$  and  $24 \text{ mg cm}^{-1} \text{ day}^{-1}$ , respectively). The nitrate loss loads due to lateral flow (2,199, 1,648, 2,140, 1,522, and 2,766 mg for the NNNN, NLLN, LHHL, LNLN, and HNHN treatments, respectively) were almost twice as those due to vertical leaching (1,123, 823, 1,128, 879, and 1,304 mg for the NNNN, NLLN, LHHL, LNLN, and HNHN treatments, respectively). This indicates that large amounts of nitrate are transported both laterally downhill and vertically towards groundwater, resulting in comparable environmental risks. Moreover, nitrate losses due to subsurface lateral flow occur mostly during rainfalls, whereas losses due to vertical leaching are incessant and less variable with time.

## 4.3 | Analysis of calibrated parameter values

The saturated hydraulic conductivity is the most important parameter for numerical simulations of water flow. The calibrated  $K_s$  value of the low permeability cement layer was a hundred times smaller than  $K_s$  of the purple soil (Table 1). Similar  $K_s$  values measured on bedrock samples were reported by Katsura, Kosugi, Yamamoto, and Mizuyama (2006). Although the low permeability layer was thin and its water storage had little effect on the overall soil storage, its hydraulic conductivity defined the leaching potential of the entire soil profile (Baram et al., 2016). The calibrated  $K_s$  of the purple soil was smaller than those reported by others (Long, Liu, & Liu, 2015) for both cultivated and uncultivated purple sloping soils. Differences in  $K_s$  were found to be dependent on the study scale (Laine-Kaulio, Backnas, Karvonen, Koivusalo, & McDonnell, 2014).  $D_L$ , which is related to the travel distance of the solute, controlled the nitrate transport. Although the thickness of the soil layer was four times larger than the thickness of the cement layer, the  $D_L$  value of the soil layer was calibrated to be about the same as that of the bedrock layer. As a result of the short duration of the experiment, the effects of the denitrification rate on nitrate decreases in the soil were insignificant during simulations.

## 5 | CONCLUSIONS

Subsurface water and nitrate leaching play an important role in water and nitrogen losses from sloped soils. It is essential to understand these losses due to subsurface lateral flow and vertical leaching and how various initial nitrate distributions can impact subsurface nitrate transport in sloped soils. In this study, HYDRUS-2D was used to analyse the subsurface nitrate transport and losses from sloped soils for five different initial nitrate distributions. HYDRUS-2D performed well when compared with experimental data, proving to be a useful modelling tool for investigating water flow and solute transport in sloped soils and for providing better interpretation of spatial and temporal dynamics of nitrate distributions and losses in such environments.

Laboratory experiments combined with the numerical analysis demonstrated that water flow was the main factor in washing  $\text{NO}_3\text{-N}$  away from the soil profile in response to rainfalls and that nitrate concentrations declined exponentially with time. Significant differences were revealed along the slope for non-uniform initial nitrate distributions. Coupled effects of elution by soil water flow and diffusion due to concentration differences on the nitrate transport were observed. Larger decreases in nitrate concentrations in the upper soil layers due to water elution were observed, whereas the effects of non-uniform distributions on  $\text{NO}_3\text{-N}$  transfer were more pronounced in the deep soil layer. Higher nitrate concentrations at the slope foot and along the slope were washed away mainly due to subsurface saturated lateral flow and vertical leaching, respectively. Non-uniform fertilizer applications at sloped soils thus need to be taken into account in order to reduce nitrate losses and keep soil fertility. Moreover, increasing nitrogen application rates enhances subsurface nitrate losses. There is thus a positive correlation between nitrate concentrations at the interface where losses occur, nitrate applications, and subsurface nitrate losses. Peak values of subsurface  $\text{NO}_3\text{-N}$  fluxes revealed that nitrate losses due to subsurface lateral flow occurred mostly during rainfall events whereas nitrate losses due to vertical leaching were more gradual and had longer duration during and after rainfalls. Average nitrate fluxes due to lateral saturated flow were twice as large as those due to vertical leaching. However, total  $\text{NO}_3\text{-N}$  fluxes due to vertical leaching (as a result of its longer duration) were comparable with those due to lateral saturated flow. Both processes thus represent comparable environmental risks to surface and groundwater.

## ACKNOWLEDGMENTS

This research was supported by the Changjiang River Scientific Research Institute and was funded by the Postgraduate Research & Practice Innovation Program of Jiangsu Province (Grant KYCX18\_0596), Fundamental Research Funds for the Central Universities (Grant 2018B627X14), National Natural Science Foundation of China (Grant 51879071), Priority Academic Program Development of Jiangsu Higher Education Institutions (Grant YS111001), and the China Scholarship Council.

## DATA AVAILABILITY STATEMENT

The data that support the findings of this study are available from the corresponding author upon reasonable request.

## ORCID

Jirka Šimůnek  <https://orcid.org/0000-0002-0166-6563>

Zhanyu Zhang  <https://orcid.org/0000-0002-7744-6698>

## REFERENCES

- Allaire, S. E., Roulier, S., & Cessna, A. J. (2009). Quantifying preferential flow in soils a review of different techniques. *Journal of Hydrology*, 378(1-2), 179–204. <https://doi.org/10.1016/j.jhydrol.2009.08.013>
- Baram, S., Couvreur, V., Harter, T., Read, M., Brown, P. H., Kandelous, M., & Hopmans, J. W. (2016). Estimating nitrate leaching to groundwater from orchards: Comparing crop nitrogen excess, deep vadose zone data-driven estimates, and HYDRUS modeling. *Vadose Zone Journal*, 15(11).
- Bechmann, M. (2014). Long-term monitoring of nitrogen in surface and subsurface runoff from small agricultural dominated catchments in Norway. *Agriculture Ecosystems & Environment*, 198(SI), 13–24. <https://doi.org/10.1016/j.agee.2014.05.010>
- Delgado, J. A., Khosla, R., Bausch, W. C., Westfall, D. G., & Inman, D. J. (2005). Nitrogen fertilizer management based on site-specific management zones reduces potential for nitrate leaching. *Journal of Soil and Water Conservation*, 60(6), 402–410.
- Doltra, J., & Munoz, P. (2010). Simulation of nitrogen leaching from a fertigated crop rotation in a Mediterranean climate using the EU-Rotate\_N and Hydrus-2D models. *Agricultural Water Management*, 97(2), 277–285. <https://doi.org/10.1016/j.agwat.2009.09.019>
- Dusek, J., Vogel, T., Dohnal, M., & Gerke, H. H. (2012). Combining dual-continuum approach with diffusion wave model to include a preferential flow component in hillslope scale modeling of shallow subsurface runoff. *Advances in Water Resources*, 44, 113–125. <https://doi.org/10.1016/j.advwatres.2012.05.006>
- Filipovic, V., Toor, G. S., Ondrasek, G., & Kodesova, R. (2015). Modeling water flow and nitrate-nitrogen transport on golf course under turfgrass. *Journal of Soils and Sediments*, 15(8), 1847–1859. <https://doi.org/10.1007/s11368-014-0980-7>
- Hamoudi, S., & Belkacemi, K. (2013). Adsorption of nitrate and phosphate ions from aqueous solutions using organically-functionalized silica materials: Kinetic modeling. *Fuel*, 110, 107–113. <https://doi.org/10.1016/j.fuel.2012.09.066>
- Jia, H., Lei, A., Lei, J., Ye, M., & Zhao, J. (2007). Effects of hydrological processes on nitrogen loss in purple soil. *Agricultural Water Management*, 89(1-2), 89–97. <https://doi.org/10.1016/j.agwat.2006.12.013>
- Kahl, G., Ingwersen, J., Nutniyom, P., Totrakool, S., Pansombat, K., Thavorniyutikarn, P., & Streck, T. (2007). Micro-trench experiments on interflow and lateral pesticide transport in a sloped soil in Northern Thailand. *Journal of Environmental Quality*, 36(4), 1205–1216. <https://doi.org/10.2134/jeq2006.0241>
- Kanthle, A. K., Lenka, N. K., Lenka, S., & Tedia, K. (2016). Biochar impact on nitrate leaching as influenced by native soil organic carbon in an Inceptisol of central India. *Soil & Tillage Research*, 157, 65–72. <https://doi.org/10.1016/j.still.2015.11.009>
- Karandish, F., & Šimůnek, J. (2017). Two-dimensional modeling of nitrogen and water dynamics for various N-managed water-saving irrigation strategies using HYDRUS. *Agricultural Water Management*, 193, 174–190. <https://doi.org/10.1016/j.agwat.2017.07.023>
- Katsura, S., Kosugi, K., Yamamoto, N., & Mizuyama, T. (2006). Saturated and unsaturated hydraulic conductivities and water retention characteristics of weathered granitic bedrock. *Vadose Zone Journal*, 5(1), 35–47. <https://doi.org/10.2136/vzj2005.0040>
- Ke, J., He, R., Hou, P., Ding, C., Ding, Y., Wang, S., & Li, G. (2018). Combined controlled-released nitrogen fertilizers and deep placement effects of N leaching, rice yield and N recovery in machine-transplanted rice. *Agriculture Ecosystems & Environment*, 265, 402–412. <https://doi.org/10.1016/j.agee.2018.06.023>
- Kleinman, P. J. A., Srinivasan, M. S., Dell, C. J., Schmidt, J. P., Sharpley, A. N., & Bryant, R. B. (2006). Role of rainfall intensity and hydrology in

- nutrient transport via surface runoff. *Journal of Environmental Quality*, 35(4), 1248–1259. <https://doi.org/10.2134/jeq2006.0015>
- Komatsu, Y., Kato, H., Zhu, B., Wang, T., Yang, F., Rakwal, R., & Onda, Y. (2018). Effects of slope gradient on runoff from bare-fallow purple soil in China under natural rainfall conditions. *Journal of Mountain Science*, 15(4), 738–751. <https://doi.org/10.1007/s11629-017-4714-3>
- Laine-Kaulio, H., Backnas, S., Karvonen, T., Koivusalo, H., & McDonnell, J. J. (2014). Lateral subsurface stormflow and solute transport in a forested hillslope: A combined measurement and modeling approach. *Water Resources Research*, 50(10), 8159–8178. <https://doi.org/10.1002/2014WR015381>
- Li, J., & Liu, Y. (2011). Water and nitrate distributions as affected by layered-textural soil and buried dripline depth under subsurface drip fertigation. *Irrigation Science*, 29(6), 469–478. <https://doi.org/10.1007/s00271-010-0255-z>
- Li, J. S., Zhang, J. J., & Rao, M. J. (2004). Wetting patterns and nitrogen distributions as affected by fertigation strategies from a surface point source. *Agricultural Water Management*, 67(2), 89–104. <https://doi.org/10.1016/j.agwat.2004.02.002>
- Li, Y., Šimůnek, J., Zhang, Z., Huang, M., Ni, L., Zhu, L., & Chen, Y. (2015). Water flow and nitrate transport through a lakeshore with different revetment materials. *Journal of Hydrology*, 520, 123–133. <https://doi.org/10.1016/j.jhydrol.2014.11.045>
- Liu, Z., Yang, J., Yang, Z., & Zou, J. (2012). Effects of rainfall and fertilizer types on nitrogen and phosphorus concentrations in surface runoff from subtropical tea fields in Zhejiang, China. *Nutrient Cycling in Agroecosystems*, 93(3), 297–307. <https://doi.org/10.1007/s10705-012-9517-x>
- Long, T., Liu, X., & Liu, J. (2015). Modeling spatial and temporal variation of nitrate loss via interflow in a sloping field of purple soil. *Journal of Agro-Environment Science*, 34(10), 1973–1978. in Chinese with English abstract
- Ma, X., Li, Y., Li, B., Han, W., Liu, D., & Gan, X. (2016). Nitrogen and phosphorus losses by runoff erosion: Field data monitored under natural rainfall in Three Gorges Reservoir Area. *China. Catena*, 147, 797–808. <https://doi.org/10.1016/j.catena.2016.09.004>
- Mualem, Y. (1976). A new model for predicting the hydraulic conductivity of unsaturated porous media. *Water Resources Research*, 12(3), 513–522. <https://doi.org/10.1029/WR012i003p00513>
- Nyamangara, J., Bergstrom, L. F., Piha, M. I., & Giller, K. E. (2003). Fertilizer use efficiency and nitrate leaching in a tropical sandy soil. *Journal of Environmental Quality*, 32(2), 599–606. <https://doi.org/10.2134/jeq2003.5990>
- Prasertsak, P., Freney, J. R., Denmead, O. T., Saffigna, P. G., Prove, B. G., & Reghenzani, J. R. (2002). Effect of fertilizer placement on nitrogen loss from sugarcane in tropical Queensland. *Nutrient Cycling in Agroecosystems*, 62(3), 229–239. <https://doi.org/10.1023/A:1021279309222>
- Russo, T. A., Tully, K., Palm, C., & Neill, C. (2017). Leaching losses from Kenyan maize cropland receiving different rates of nitrogen fertilizer. *Nutrient Cycling in Agroecosystems*, 108(2), 195–209. <https://doi.org/10.1007/s10705-017-9852-z>
- Salehi, A. A., Navabian, M., Varaki, M. E., & Pirmoradian, N. (2017). Evaluation of Hydrus-2D model to simulate the loss of nitrate in subsurface controlled drainage in a physical model scale of paddy fields. *Paddy and Water Environment*, 15(2), 433–442. <https://doi.org/10.1007/s10333-016-0561-z>
- Schaap, M. G., Leij, F. J., & van Genuchten, M. T. (1998). Neural network analysis for hierarchical prediction of soil hydraulic properties. *Soil Science Society of America Journal*, 62(4), 847–855. <https://doi.org/10.2136/sssaj1998.03615995006200040001x>
- Schneider, A., Baumgartl, T., Doley, D., & Mulligan, D. (2010). Evaluation of the heterogeneity of constructed landforms for rehabilitation using lysimeters. *Vadose Zone Journal*, 9(4), 898–909. <https://doi.org/10.2136/vzj2009.0172>
- Šimůnek, J., van Genuchten, M. T., & Šejna, M. (2008). Development and applications of the HYDRUS and STANMOD software packages and related codes. *Vadose Zone Journal*, 7(2), 587–600. <https://doi.org/10.2136/vzj2007.0077>
- Šimůnek, J., van Genuchten, M. T., & Šejna, M. (2016). Recent developments and applications of the HYDRUS computer software packages. *Vadose Zone Journal*, 15(7).
- Smith, D. R., Owens, P. R., Leytem, A. B., & Warnemuende, E. A. (2007). Nutrient losses from manure and fertilizer applications as impacted by time to first runoff event. *Environmental Pollution*, 147(1), 131–137. <https://doi.org/10.1016/j.envpol.2006.08.021>
- Sweeney, D. W., Pierzynski, G. M., & Barnes, P. L. (2012). Nutrient losses in field-scale surface runoff from claypan soil receiving turkey litter and fertilizer. *Agriculture Ecosystems & Environment*, 150, 19–26. <https://doi.org/10.1016/j.agee.2012.01.008>
- Tang, J., Zhu, B., Wang, T., Cheng, X., Gao, M., & Lin, H. (2012). Subsurface flow processes in sloping cropland of purple soil. *Journal of Mountain Science*, 9(1), 1–9. <https://doi.org/10.1007/s11629-012-2199-7>
- van Genuchten, M. T. (1980). A closed-form equation for predicting the hydraulic conductivity of unsaturated soils 1. *Soil Science Society of America Journal*, 44(5), 892–898. <https://doi.org/10.2136/sssaj1980.03615995004400050002x>
- Wang, H., Ping, L., Pan, J., & Shen, Z. (2012). Effects of solute application position on the solute transport characteristics on red soil slope. *Journal of Soil and Water Conservation*, 26(4), 7–11.
- Wang, Q., Li, F., Zhao, L., Zhang, E., Shi, S., Zhao, W., & Vance, M. M. (2010). Effects of irrigation and nitrogen application rates on nitrate nitrogen distribution and fertilizer nitrogen loss, wheat yield and nitrogen uptake on a recently reclaimed sandy farmland. *Plant and Soil*, 337(1–2), 325–339. <https://doi.org/10.1007/s11104-010-0530-z>
- Wang, Y., Ying, H., Yin, Y., Zheng, H., & Cui, Z. (2018). Estimating soil nitrate leaching of nitrogen fertilizer from global meta-analysis. *The Science of the total environment*, 657, 96–102.
- Wang, Y., Zhang, B., Lin, L., & Zepp, H. (2011). Agroforestry system reduces subsurface lateral flow and nitrate loss in Jiangxi Province. *China. Agriculture Ecosystems & Environment*, 140(3–4), 441–453. <https://doi.org/10.1016/j.agee.2011.01.007>
- Wang, Z., Zhang, T. Q., Tan, C. S., Taylor, R. A. J., Wang, X., Qi, Z. M., & Welacky, T. (2018). Simulating crop yield, surface runoff, tile drainage and phosphorus loss in a clay loam soil of the Lake Erie region using EPIC. *Agricultural Water Management*, 204, 212–221. <https://doi.org/10.1016/j.agwat.2018.04.021>
- Wu, L., Peng, M., Qiao, S., & Ma, X. (2018). Effects of rainfall intensity and slope gradient on runoff and sediment yield characteristics of bare loess soil. *Environmental Science and Pollution Research*, 25(45), 3480–3487. <https://doi.org/10.1007/s11356-017-0713-8>
- Xie, M., Zhang, Z., Zhang, P., & Chen, T. (2018). Nitrate nitrogen transport and leaching from sloping farmland of purple soil: Experimental and modelling approaches. *Fresenius Environmental Bulletin*, 27(3), 1508–1521.
- Xie, M., Zhang, Z., Zhang, P., Xu, J., & Lin, Q. (2018). Law of nitrate transfer and loss in purple sloping farmland and its numerical simulation. *Transactions of the Chinese Society of Agricultural Engineering*, 34(19), 147–154. in Chinese with English abstract
- Xu, L., Niu, H., Xu, J., & Wang, X. (2013). Nitrate-nitrogen leaching and modeling in intensive agriculture farmland in China. *Scientific World Journal*, 2013, 353086.
- Zhang, B., Tang, J. L., Gao, C., & Zepp, H. (2011). Subsurface lateral flow from hillslope and its contribution to nitrate loading in streams

- through an agricultural catchment during subtropical rainstorm events. *Hydrology and Earth System Sciences*, 15(10), 3153–3170. <https://doi.org/10.5194/hess-15-3153-2011>
- Zhao, Y., & Shao, M. (2002). Experimental study on nitrate transport for different fertilization methods. *Transactions of the CSAE*, 18(4), 37–40.
- Zheng, H., Liu, Z., Zuo, J., Wang, L., & Nie, X. (2017). Characteristics of nitrogen loss through surface-subsurface flow on red soil slopes of Southeast China. *Eurasian Soil Science*, 50(12), 1506–1514. <https://doi.org/10.1134/S1064229317130063>
- Zhu, B., Wang, T., Kuang, F., Luo, Z., Tang, J., & Xu, T. (2009). Measurements of nitrate leaching from a hillslope cropland in the central Sichuan Basin, China. *Soil Science Society of America Journal*, 73(4), 1419–1426. <https://doi.org/10.2136/sssaj2008.0259>

**How to cite this article:** Xie M, Šimůnek J, Zhang Z, Zhang P, Xu J, Lin Q. Nitrate subsurface transport and losses in response to its initial distributions in sloped soils: An experimental and modelling study. *Hydrological Processes*. 2019;1–15. <https://doi.org/10.1002/hyp.13556>